

Investigation of vegetation dynamics with a focus on agricultural land cover and its relation with meteorological parameters based on the remote sensing techniques: a case study of the Gavkhoni watershed**

Iman Rousta^{1,2} , Safoora Izadian¹, Haraldur Olafsson², Anna Siedliska³ , and Jaromir Krzyszczak³ *

¹Department of Geography, Yazd University, Yazd 8915818411, Iran

²Institute for Atmospheric Sciences-Weather and Climate and Department of Physics, University of Iceland and Icelandic Meteorological Office (IMO), Bustadavegur 7, IS-108 Reykjavik, Iceland

³Institute of Agrophysics, Polish Academy of Sciences, Doświadczalna 4, 20-290 Lublin, Poland

Received January 31, 2024; accepted March 12, 2024

Abstract. Background and Aims: This research investigates vegetation dynamics in the Gavkhouni catchment from 2001 to 2021, focusing on the spring season. The aim is to analyse the relationship between aridity, vegetation, and rainfall. Moreover, additional emphasis was placed on exploring the impact of these dynamics on agricultural land cover thereby contributing to our understanding of the environmental dynamics in the Gavkhouni catchment. Methods: The study made use of MODIS data, including the Enhanced Vegetation Index and Vegetation Condition Index, along with monthly rainfall statistics from Chirps. Analytical methods include time series analyses using correlation and regression analysis. Results: Throughout the study period, the average spring vegetation cover was 9276.33 km². The years 2001 and 2018 had the lowest degree of vegetation (15.53, and 17.3% of the watershed area). Conversely, 2013, 2019, and 2020 had the most coverage (27.4, 26.8, and 26.3%). The Enhanced Vegetation Index highlighted the arid years (2001, 2008, 2011, and 2018) and the years with the lowest drought prevalence (2006, 2007, 2010, 2013). Enhanced Vegetation Index correlated with spring rainfall. Cropland cover declined over the study period, and a close correlation was found between winter rainfall and spring agricultural coverage.

Keywords: vegetation, agriculture, Gavkhouni watershed, precipitation, remote sensing

1. INTRODUCTION

Investigations dealing with vegetation coverage fluctuations constitute an important area of study for vegetation management and control that aligns with the principles of sustainable development. The pivotal role of vegetation within the ecosystem is a well-established fact acknowledged by researchers (Gupta *et al.*, 2020; Peng *et al.*, 2012) as it facilitates energy exchange, water circulation, and biogeochemical cycles on the Earth's surface. Indeed, the capacity of vegetation to influence habitat conditions and species composition represents a significant area of interest within the biological sciences (Rannow and Neubert, 2014).

Remote sensing has emerged as an efficacious approach for quantifying the influence of climate and topography on spatial vegetation patterns (Couteron *et al.*, 2014). By discerning vegetation-specific radiation, this technology facilitates the discernment of changes in plant reflection (Manesh *et al.*, 2018). Employing satellite data to monitor extensive plant activities has distinct advantages over conventional methods (Pei *et al.*, 2018). Over recent decades, the significance of indicators such as Normalized Difference Vegetation Index (NDVI) and Enhanced Vegetation Index (EVI) with reference to the areas of vegetation dynamics,

*Corresponding author e-mail: j.krzyszczak@ipan.lublin.pl

**This work was supported by Vedurfelagid, Rannis and Rannsoknastofa i vedurfrædi.

drought monitoring, and evaluation have been repeatedly described (Olafsson and Rousta, 2021; Wan *et al.*, 2004). The *EVI*, an enhanced NDVI, is calculated using MODIS sensor data and constitutes valuable time series data, and is indispensable for monitoring global vegetation dynamics (Ghafarian Malamiri *et al.*, 2018). Relevant studies have demonstrated that climate plays a dominant and controlling role as an environmental factor. In particular, its two primary parameters, temperature and precipitation, significantly influence the distribution of vegetation types within terrestrial ecosystems and contribute to their temporal and spatial diversity. These effects occur on both global and local scales (Chang *et al.*, 2014; Luan *et al.*, 2018; Reynolds *et al.*, 2008; Zhong *et al.*, 2010). Precipitation is a particularly important climate parameter, having a significant influence over vegetation dynamics within arid and semi-arid ecosystems (Martiny *et al.*, 2006; Rousta *et al.*, 2014). Moreover, precipitation directly impacts the water balance and serves as a significant factor in altering soil moisture and influencing plant growth (Farajzadeh *et al.*, 2011). Ground-truth data for validating and calibrating satellite-derived estimates are provided through the use of stationary measurements of soil moisture. These measurements involve the use of in-situ sensors such as time domain reflectometry (TDR) probes, capacitance sensors, or neutron probes to monitor moisture changes within the soil profile at specific locations over time (Majcher *et al.*, 2021). By capturing moisture dynamics at different depths, stationary measurements offer insights into vertical water movement, root zone moisture distribution, and soil moisture variability across various landscapes (Kafarski *et al.*, 2019). However, at the present time drought and flood monitoring is often based on remote sensing rainfall images provided by satellites as a viable substitute for conventional measurements and meteorological data (Gupta *et al.*, 2020; Rousta *et al.*, 2018).

In recent years, drought has emerged as a prevalent and critical natural disaster and climatic phenomenon. It exerts profound impacts on communities, water resources, and ecosystems (Bhuiyan *et al.*, 2006; Dorjsuren *et al.*, 2016; Rousta *et al.*, 2017; Zhang *et al.*, 2013). Numerous researchers have emphasized that the most crucial factor driving changes in vegetation is drought and the variations resulting from shifts in rainfall patterns (Farahani *et al.*, 2022). The consequences of drought are especially severe for agricultural communities that depend on water resources, by contrast non-agricultural communities aren't so severely affected. Since the rural economy in many developing countries relies heavily on agriculture, and this agriculture is solely dependent on rainfall, the impact of drought is even more pronounced in such cases (Ashraf and Routray, 2013). In meteorological terms, drought manifests as a period marked by below-average rainfall, this results in a temporary shift in weather patterns. Subsequently, contingent upon soil moisture levels, agricultural drought ensues

and also, if prolonged, hydrological drought that diminishes river flow and other water reservoirs. The ultimate result of a prolonged lack of rainfall encompasses economic drought, which imposes detrimental consequences upon both society and the environment (Mansourmoghaddam *et al.*, 2022). As a consequence, based on the influence of distinct environmental factors, drought can be classified into meteorological, agricultural, hydrological, and socio-economic subtypes (Peters, 2003; Tate and Gustard, 2000).

The Gavkhouni watershed is a part of the watershed of the Central Plateau of Iran, it exhibits a diverse array of climate patterns, ranging from exceedingly dry to substantially humid owing to its altitude range between 1466 to 3974 m. This basin is classified as being exceptionally important due to its size and location in central Iran and also the availability of suitable soils for agriculture. The existence of about 70 cities and 1720 villages in the region, the presence of the metropolis of Isfahan, the existence of the Gavkhouni wetland and the Zayandeh Roud watershed further accentuate its significance. In recent years, climate change and diminished precipitation have resulted in the permanent depletion of Zayandeh Roud's flow and in the desiccation of the ecologically vital Gavkhouni wetland (Mirahsani *et al.*, 2018). To date, these areas have been preserving biodiversity, controlling fine dust and air pollution, impacting local, provincial, regional, national, and transnational climate/temperature equilibrium, and influencing the living conditions in Central Iran. As a consequence, such topics as climate and weather regulation, maintaining the stable flow of the Zayandeh Roud from Sarab to Payab, hydrological control and protection, water resource quality and production, groundwater replenishment, soil erosion prevention, as well as various economic and social dimensions, including tourism, agriculture (Jafari and Bakhshandehmehr, 2016), animal husbandry, food production, employment, green economy development, the livelihood of local communities, disease prevention, health maintenance and meeting consumption needs are emerging as focal areas of concern. This applies especially in the central and eastern regions, the negative impact on the regional economy in general and agriculture in particular, and also the well-being of numerous animals and birds, cannot be overlooked. Thus, a comprehensive investigation into droughts and climate change in this region is indispensable.

Given the dry and semi-arid climate prevalent in Central Iran and the varying rainfall distribution across different areas of the basin (northern and western sections exhibit increased rainfall due to higher altitudes), assessing the processes leading to changes in vegetation relative to basin rainfall acquires significance from the viewpoint of ecological sustainability. Increased vegetation cover yields benefits such as carbon dioxide reduction, enhanced air quality, soil moisture preservation, water and soil conservation, and flood mitigation, these are all integral to ecological stability. By contrast, environmental instability

may lead to desertification, soil erosion (Weishou *et al.*, 2011), climate change, and other issues, inflicting adverse economic, social, and climatic consequences. As drought is a prime factor contributing to vegetation reduction, this further underscores the importance of the subject under investigation, with climate changes and atmospheric circulation shifts serving as underlying causative agents (Khosravi *et al.*, 2023).

Also, changes in climate, including the precipitation occurring over the last few decades, are important in terms of being one of the factors affecting the reduction in soil resources and in the low levels of water found in rivers. The dependence of the agricultural sector on water is undeniable. The rural employment rate in the agriculture sector in the Gavkhouni watershed is 89%, so this basin is known as one of the agricultural poles in the basins of Iran and is very important (Sarai *et al.*, 2017).

In this study, the Enhanced Vegetation Index (*EVI*), Vegetation Condition Index (*VCI*), and Standardized Precipitation Index (*SPI*) were used to reveal drought occurrences and vegetation area changes across different zones within the basin throughout the period spanning from 2001 to 2021. Special attention was focused on agricultural land cover in order to assess its dynamics and the degree of interdependence with climatic variables.

2. MATERIALS AND METHODS

2.1. Study area

The Gavkhouni watershed area spans 41 552.3 km² and is located at an elevation of 1 450 m above sea level. From the viewpoint of the general division of Iran's hydrology, the Gavkhouni watershed is an integral component of the

Central Plateau of Iran's broader watershed system, it is bordered by the Namak Lake watershed to the north, the Degh Sohrh and Siahkouh desert basins to the east, the Abarqo desert basin to the south, and the Karun watershed to the west and south. It is notable that a significant portion, constituting 83% of the Gavkhouni International Lagoon catchment area, falls within the Isfahan province, while 9% extends into Fars province, 4.5% into Chaharmahal and Bakhtiari province, and 3.5% into the Yazd province. More than two-thirds of the Gavkhouni watershed area belongs to the Zayandeh Roud basin, which encompasses an area of 26 917 km². This region is of major importance due to the establishment of major population centres there, industrial developments, and the primary concentration of agricultural activities within the Gavkhouni basin. The geographic coordinates of the basin fall between 50°2' to 53°24' east and 31°12' to 33°42' north and the elevation ranges from 1 450 to 3 900 m above sea level (Fig. 1).

2.2. Data and methodology

The land cover map utilized in this study (Fig. 2) is the MCD12Q1 annual product (IGBP) acquired from the MODIS system, it was obtained from the United States Geological Survey website (<https://Ipdaacsvc.cr.usgs.gov/appears/task/area>). This map, embracing 17 distinct classes, meticulously characterizes the surface cover across the Earth (Belward *et al.*, 1999; Loveland and Belward, 1997). For the period spanning from 2001 to 2021, the land cover within the Gavkhouni watershed is delineated into 7 discrete classes, designated as classes 7, 9, 10, 12, 13, 16, and 17, in accordance with the classification scheme devised by the University of Maryland (Hansen *et al.*, 2000). These

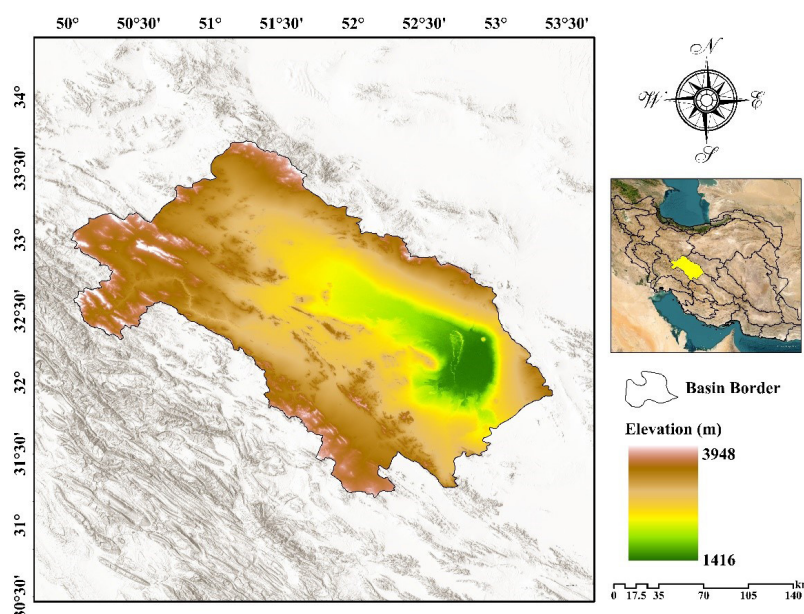


Fig. 1. Geographical location of the Gavkhouni watershed between the sub-basins of Iran (right), and a digital elevation model (DEM) map of the Gavkhouni watershed.

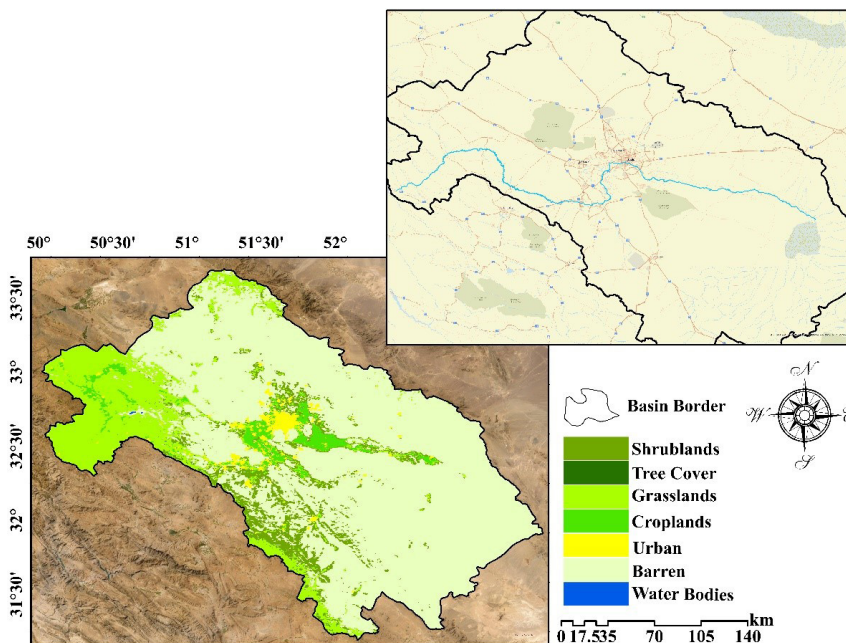


Fig. 2. Land cover map of the Gavkhouni watershed (overview map created for 2010).

classes correspond, respectively, to shrubland, tree cover (canopy exceeding 2 m in height), grassland, agricultural land, urban and man-made areas, bare land, and wetland areas. As illustrated in Fig. 2, the vegetation within the Gavkhouni catchment basin is predominantly represented by shrubland and grassland (pasture) formations, occupying central, northwestern, and western sectors of the basin, where the extent of the vegetation coverage corresponds to the elevated regions. The Digital Elevation Map (DEM) data was made using USGS EarthExplorer data (<https://earthexplorer.usgs.gov/>).

For this study, a dataset consisting of 484 *EVI* images, derived from Moderate Resolution Imaging Spectroradiometer (MODIS), was compiled for the Gavkhouni watershed, the dataset spanned a period of 21 years (2001–2021). The MOD13Q1 MODIS sensor offers a spatial resolution of 250 m, a radiometric resolution of 12 bits, and a spectral range of 0.4 to 14.4 μm . Moreover, it provides observations at various temporal resolutions, including daily, 4-day, 8-day, 16-day, quarterly, and annual intervals. The *EVI* images were extracted from MODIS sensor observations at a 250 m spatial resolution, they were acquired every 16 days using the Google Earth Engine system. The periods were partitioned as follows: the winter vegetation data was derived from an average of 6 images ranging from image number 353 to 065, corresponding to a period ranging from December 19 to March 6; the spring vegetation data was derived from an average of 6 images spanning from image 081 to 161, this corresponds to the period of March 22 to June 10; the summer vegetation data was derived from an average of 6 images

spanning from image 177 to 257, it encompassed June 26 to September 14; the autumn vegetation data was calculated from an average of 5 images ranging from 273 to 337, it corresponded to September 30 to December 3; and the annual vegetation data was obtained from an average of 23 images ranging from 017 to 001, representing January 17 of the preceding year to January 1 of the subsequent year. In the next step, 251 monthly images of precipitation were downloaded and processed. The total annual rainfall was calculated as the sum of precipitation across all 12 months, while seasonal rainfall data was determined for winter (December, January, and February), spring (March, April, and May), summer (June, July, and August), and autumn (September, October, and November). The seasonal and annual *EVI*, *VCI*, and precipitation images were processed using the ArcGIS environment. Subsequently, all pixel values for daily, seasonal, and annual datasets were imported into EXCEL software, where extensive analysis, classification, graph plotting, inter-indicator correlations, and assessments of changes in precipitation and vegetation were conducted. Additionally, vegetation area calculations were performed using this software. Then, the cropland class was extracted separately from the landcover maps of each year and checked according to the average spring season maps of the basin.

Also, the Chirps rainfall dataset was employed to assess precipitation patterns. The Chirps data encompasses the region between 50°N and 50°S, it spanned all longitudes, with temporal coverage extending from the commencement of January 1981 to the present day, with daily, monthly, and seasonal values. The CHIRPS product is a compilation

of over thirty years of global rainfall data, with a spatial resolution of approximately 0.05° on a global scale. This product utilizes not only satellite information but is also validated by ground stations, thereby making it a widely employed resource for drought monitoring. These images were obtained monthly during the period ranging from 2001 to 2021 via the website <https://www.chc.ucsb.edu/data/chirps>. Subsequently, they were extracted on a quarterly and annual basis within the ArcGIS environment.

2.3. Enhanced Vegetation Index (EVI)

The *EVI* has been developed as an advancement over the *NDVI*, the aim is to optimize vegetation signals within the leaf surface index range. By incorporating the blue band reflection to mitigate soil background signals and account for atmospheric effects, including the dispersion of suspended particles, the *EVI* demonstrates superior performance (Huete *et al.*, 1994). The mathematical formulation of the *EVI* is represented as:

$$EVI = G \left(\frac{B_{NIR} - B_{RED}}{B_{NIR} + C_1 B_{RED} - C_2 B_{BLUE} + L} \right). \quad (1)$$

Here, B_{NIR} , B_{RED} , and B_{BLUE} denote the near-infrared band, red band, and blue band, respectively. L serves as the land and soil adjustment factor, it is set to 1. The coefficients C_1 and C_2 are utilized for correcting aerosol dispersion. Notably, in the red bands, the values of C_1 and C_2 are equal to 6 and 7.5, respectively. The weight factor G , which was set at 2.5, further enhances the performance of the *EVI* (Huete *et al.*, 1994, 1997, 1999, 2002). The annual and seasonal improved *EVI* was calculated as follows:

$$\text{Winter vegetation coverage} = \frac{\sum(\text{image 353 to image 065})}{6}, \quad (2)$$

$$\text{Spring vegetation coverage} = \frac{\sum(\text{image 081 to image 161})}{6}, \quad (3)$$

$$\text{Summer vegetation coverage} = \frac{\sum(\text{image 177 to image 257})}{6}, \quad (4)$$

$$\text{Fall vegetation coverage} = \frac{\sum(\text{image 273 to image 337})}{5}, \quad (5)$$

$$\text{Yearly vegetation coverage} = \frac{\sum(\text{image 017 to image 001})}{23}. \quad (6)$$

2.4. Standardized Precipitation Index (SPI)

The *SPI* constitutes a prominent method utilized for drought assessment and is formulated as follows:

$$SPI = \frac{x_i - x_m}{SD}. \quad (7)$$

In the relationship above, x_i denotes the amount of precipitation for each month, season, or year, x_m represents the average precipitation observed during the statistically

Table 1. Classification of wet and dry periods according to the Standard Precipitation Index (*SPI*)

Description	Class
Extremely wet	≥ 2
Very wet	1.5 – 2
Moderately wet	1 – 1.5
Near normal	-1 – 1
Moderate drought	-1.5 – -1
Severe drought	-2 – -1.5
Extreme drought	≤ -2

relevant period, and SD denotes the standard deviation observed during that period. A comprehensive interpretation of the *SPI* results is presented in Table 1, where positive values indicate rainfall which surpasses the average, whereas negative values suggest the opposite scenario (Cancelliere *et al.*, 2007; Shah *et al.*, 2015).

2.5. Vegetation Condition Index (VCI)

The concept of the *VCI* was initially introduced by Kogan in 1995 (Kogan, 1995). The *VCI* is computed and standardized against a range of long-term *NDVI* values. The *NDVI* is derived from the contrast between the red and near-infrared bands within an image, thereby providing valuable insights into the vegetation percentage, plant photosynthetic activity, surface water presence, leaf area index, and biomass quantity. This index is assigned values within the range of -1 to 1. As the *EVI* represents an enhancement of the *NDVI*, it has also been used for *VCI* computation. The numerical output of the *VCI* index is expressed as a percentage within the range of 0 to 100. Values nearing zero signify the presence of stress and severe drought in the region, whereas values approaching 100 indicate favourable vegetation conditions with no water stress (Kogan, 1997). It is calculated as follows:

$$VCI = \left(\frac{EVI - EVI_{min}}{EVI_{max} - EVI_{min}} \right) 100. \quad (8)$$

In the relationship above, *EVI* denotes the improved seasonal or annual vegetation cover index, whereas EVI_{min} and EVI_{max} denote the minimum and maximum long-term *EVI* values observed across the entire study area during the period spanning from 2001 to 2021, respectively.

3. RESULTS

3.1. Temporal and spatial changes in vegetation

From the results presented in Fig. 3, it is evident that the Gavkhouni catchment area exhibits the most extensive vegetation area during the spring season. The period of robust vegetation growth commences on late March, this extends

throughout the entirety of the summer, with peak vegetation cover in the region occurring on the beginning of May, accounting for 27.35% of the total area (11363.8 km²). Subsequently, from late June onward, the vegetation undergoes a gradual decline, but it persists until the conclusion of winter. The winter season in general, but culminating on the middle of January, records the lowest vegetation area at 5.1% (2130 km²). It is evident that the observed decline in vegetation area during the summer season, which includes the period from late June to the middle of September, is concurrent with the drying of vegetation experienced in this season. This phenomenon results in diminished vegetation coverage as compared to the flourishing conditions observed during the spring season. Additionally, the relative humidity of the air plays a significant role, as it exhibits a positive correlation with the rate of water evaporation from both the leaf surfaces and the ground. Consequently, not only does this favour an augmented water supply to the plants in the soil, but it also reduces the daily water requirement of the plants (Rousta *et al.*, 2020a). In the summer season, only green trees and parks in urban areas and at higher altitudes manage to preserve their vegetation due to reduced temperatures, this leads to decreased evaporation and transpiration rates in these plants within the studied area.

Based on the findings presented in Fig. 4, it is evident that the spring season demonstrates the most substantial vegetation in terms of its extent, encompassing an average area of 9276.3 km². Subsequently, the summer season follows suit with the largest vegetation area after spring, covering 6986.36 km² it is the largest area of vegetation among the seasons after the spring season. Conversely, during the autumn season, the vegetation area undergoes a reduction due to the complete evaporation of water from the leaves of dry trees, with an average area of 3710.03 km² observed, it is mainly poor vegetation (*EVI* from 0.1 to 0.2), with limited occurrences confined primarily to urban areas and the northwest and west elevations. In the winter season, as the catchment area experiences increased rainfall, particularly in the northwest and west elevations, and reduced air temperatures, the vegetation area in these regions diminishes to zero. Moreover, the vegetation cover during this season remains scant in the centre of the basin, but relatively more concentrated in urban areas, occupying an area of 2485.64 km². Figure 4 offers a comprehensive depiction of the average vegetation cover fluctuations across the four distinct seasons.

Figure 5 illustrates the temporal dynamics of vegetation cover as measured by the *EVI* throughout the period in the Gavkhouni catchment area. Within this figure, positive values displayed in green signify increments in vegetation cover, whereas negative values displayed in red indicate reductions in vegetation during the specified period. Areas characterized by intermediate values and represented in white denote regions with no significant vegetation

changes. A notable observation from the figure reveals green areas, they signify an upward trend in vegetation cover, predominantly situated in the northwest, west, in certain central areas, and to a lesser extent in the northeast and southwest regions, extending southwards within the Gavkhouni catchment area. Additionally, scattered instances of increasing vegetation cover are evident within

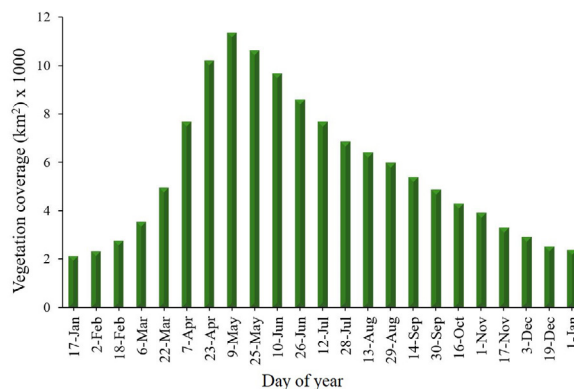


Fig. 3. Average vegetation cover in the Gavkhouni catchment during the period of 2001-2021.

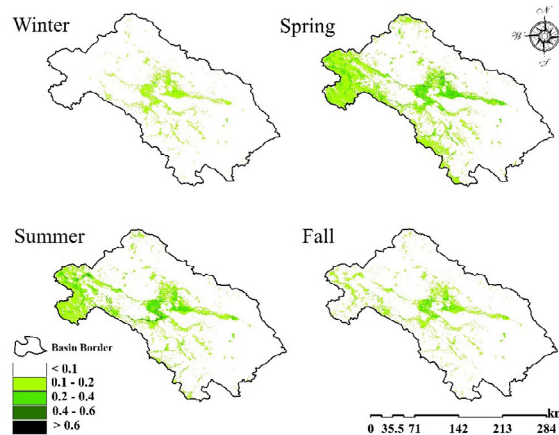


Fig. 4. Average vegetation cover changes from spring to winter during the period of 2001-2021.

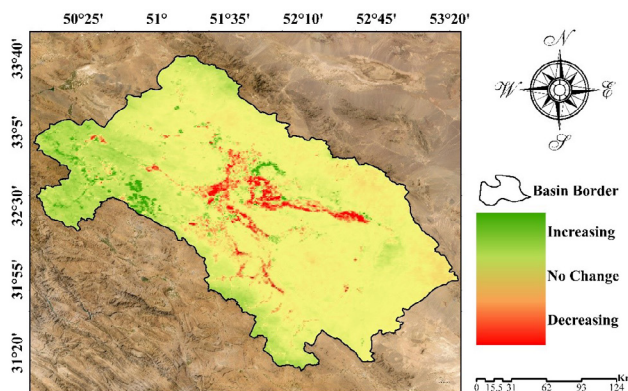


Fig. 5. Trends in *EVI* changes in the Gavkhouni catchment during the period of 2001-2021.

the central basin, they are particularly concentrated around urban areas. Conversely, the most substantial decrease in vegetation cover is observed at the centre of the Gavkhouni catchment area, further extending towards the southwest and southeast regions. Notably, the white areas indicate a trend of unchanged vegetation cover, attesting to the achievement of stability during the study period.

3.2. Results of vegetation change evaluation

The variations in vegetation area across different seasons during the statistical study period were also investigated. In the present study, the investigations focused on the vegetation area of the spring season because in this season the highest level of vegetation coverage was recorded. The results revealed that throughout the study period, the spring seasons of 2001, 2002, 2008, and 2018 produced the lowest vegetation cover, accounting for 15.53, 17.8, 18.39, and 17.3% of the Gavkhouni catchment area, respectively (Table 2). Conversely, the region also encountered wetter years, such as 2006, 2007, 2010, 2013, 2019, and 2020, where vegetation coverage reached 25.19, 25.9, 28.2, 27.4, 26.8, and 26.3% of the total study area, respectively. Table 2 provides insights into the variations within the different layers of the *EVI* coverage in

the Gavkhouni catchment basin during the spring season throughout the period from 2001 to 2021. Based on distinct vegetation classes, an *EVI* range of 0.1 to 0.2 exhibited a significant increasing trend ($R = 0.5$), an *EVI* range of 0.2 to 0.4 displayed no significant trend, while an *EVI* range of 0.4 to 0.6 demonstrated a significant decreasing trend during the study period, *EVI* values exceeding 0.6 also showed a decreasing trend. In Fig. 6 the temporal changes in spring coverage across different classes are presented, thereby emphasizing that the maximum area of poor vegetation (0.1-0.2) was recorded in 2019, it encompassed 9156.86 km², whereas the minimum area was observed in 2001, totalling 5003.42 km². The moderate vegetation level (0.2-0.4) was highest in 2010, covering an area of 3010.23 km², and the lowest in 2001, with 1363.43 km². Good vegetation (0.4-0.6) reached its peak in 2006, it encompassed 584.65 km², while the lowest extent was found in 2018, with 52.37 km². Lastly, the extensive vegetation (*EVI* more than 0.6) peaked in 2004, covering 7.13 km², while the smallest areas were recorded in 2001 and 2011, at 0.77 km². The 21-year average area for each vegetation class is 7050.7, 2025.7, 197.39, and 2.42 km², respectively.

Table 2. Area of coverage (km²) of different *EVI* classes in the spring season in the Gavkhoni catchment area during the period of 2001-2021

Year	<i>EVI</i>				Total area
	0.1-0.2	0.2-0.4	0.4-0.6	> 0.6	
2001	5003.42	1363.43	84.92	0.77	6452.57
2002	5746.90	1540.47	128.75	1.31	7417.48
2003	6042.47	1998.28	282.10	3.70	8326.54
2004	6564.16	2141.42	407.72	7.13	9120.41
2005	6361.25	2178.76	317.00	1.53	8858.53
2006	7338.13	2540.73	584.65	6.78	10470.29
2007	7967.50	2469.00	353.25	3.17	10792.93
2008	5239.83	2196.50	207.33	0.99	7644.68
2009	6892.90	2036.15	113.5	0.90	9043.62
2010	8449.59	3010.23	292.33	2.43	11754.57
2011	6353.76	1636.97	80.76	0.77	8072.26
2012	6934.12	1757.25	83.29	0.59	8775.24
2013	9079.56	2181.73	126.64	1.80	11389.73
2014	7318.46	1812.40	94.79	1.94	9227.58
2015	7557.74	2176.47	184.40	2.70	9921.51
2016	7208.16	2246.71	228.83	3.51	9687.21
2017	7526.00	1970.51	122.20	1.62	9620.36
2018	5651.00	1523.17	52.37	0.90	7227.52
2019	9156.86	1870.26	120.51	4.92	11152.53
2020	8475.42	2245.71	206.46	2.52	10930.18
2021	7199.07	1643.83	73.39	0.81	8917.10
Average	7050.70	2025.70	197.39	2.42	9276.33

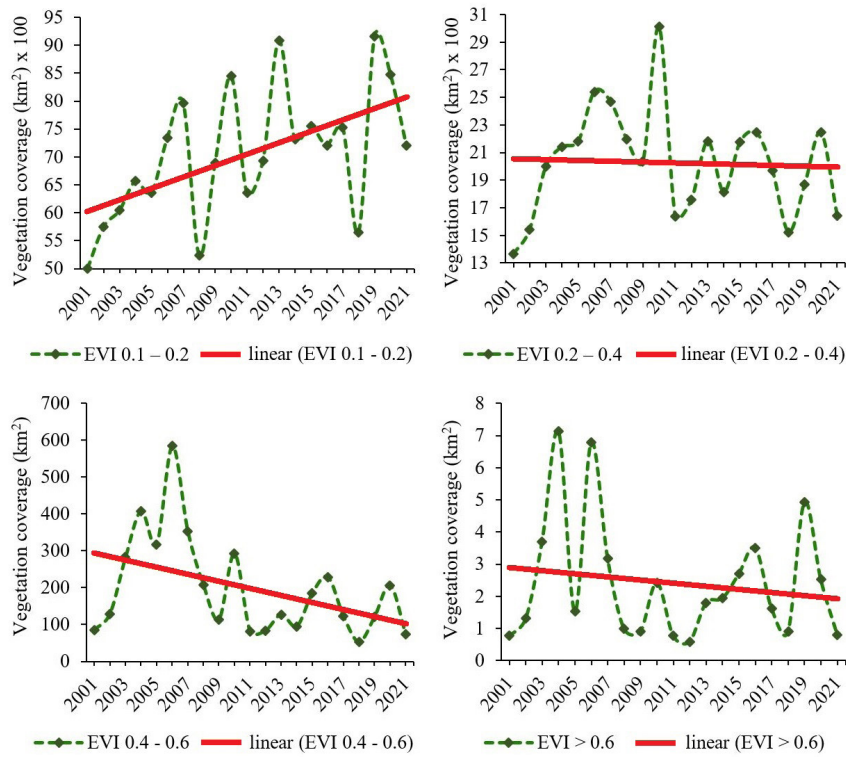


Fig. 6. Time series of different *EVI* classes for the Gavkhouni catchment during the period of 2001-2021.

In Figure 7, the relationship between spring vegetation and drought severity, which was computed using the *EVI* and the *VCI* in the Gavkhouni catchment area during the period spanning from 2001 to 2021, is presented. Drought areas, as delineated in the research conducted by Dikici (2022) are characterized by values ranging from 0 to 37.5, whereas areas without drought are identified by values exceeding 37.5. Within the entirety of the Gavkhouni

catchment area, the spring season produces fluctuations each year, with an average vegetation area of 9276.3 km² (accounting for 22.32% of the total study area) during the entire period under examination. As indicated by the *VCI* index, the years 2001, 2008, 2011, and 2018 exhibit the highest levels of drought severity, representing 83.4, 78.9, 68.3, and 79.3% of the total catchment area, respectively. Conversely, the lowest percentages of drought areas were

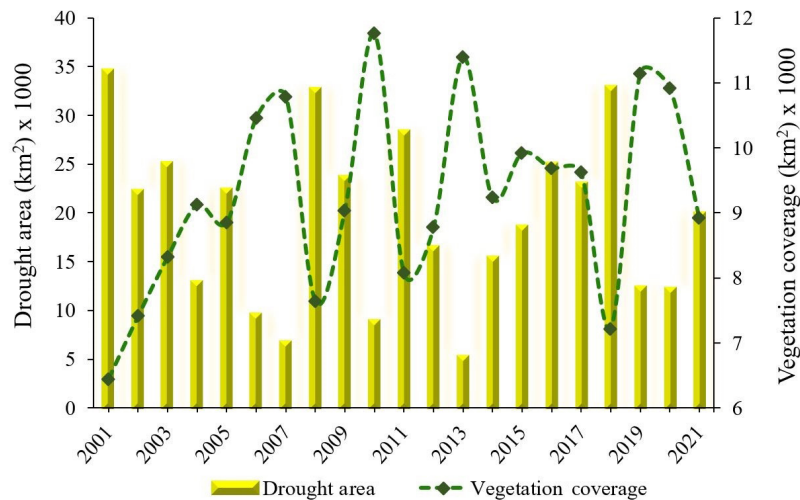


Fig. 7. Distribution of vegetation area and dry area in the Gavkhouni catchment during the period of 2001-2021.

Table 3. Correlation of the area of different *EVI* classes with the dry area in the Gavkhoni catchment during the statistical period of 2001-2021

	<i>EVI</i>				Total area
	0.1-0.2	0.2-0.4	0.4-0.6	> 0.6	
Dry area	-0.638**	-0.419**	-0.305	-0.335*	-0.667**

Correlation significant at: *p = 0.05 and **p = 0.01.

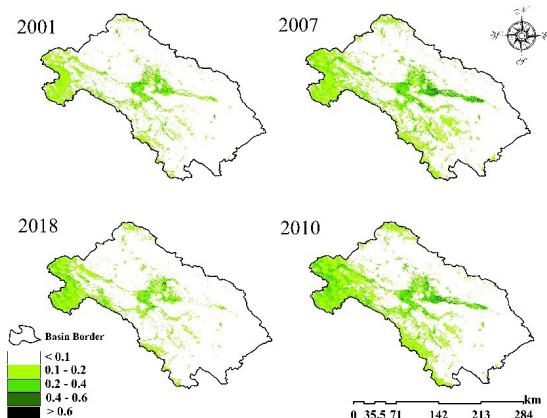


Fig. 8. Maps of spring *EVI* during dry (2001 and 2018, left panels) and wet (2007 and 2010, right panels) years in the Gavkhoni watershed.

observed during the years 2006, 2007, 2010, and 2013, amounting to 23.1, 16.2, 21.4, and 12.6% of the total area, respectively.

In contrast to the *VCI*, the *EVI* exhibits its lowest extent during the years 2001, 2002, 2008, 2011, and 2018, constituting 15.53, 17.85, 18.39, 19.42, and 17.39% of the total area, respectively. This noteworthy finding underscores a notably strong negative correlation (-0.667) between the two aforementioned indices, with the statistical significance at the 0.01 level. Table 3 offers insights into the correlation of various *EVI* classes with the area affected by dry conditions. The areas covered by poor vegetation (0.1 to 0.2) and moderate vegetation (0.2 to 0.4) demonstrate a significant negative correlation with the dry area at p=0.01. On the other hand, good vegetation (0.4 to 0.6) exhibits a negative trend without statistical significance, while extensive vegetation (exceeding 0.6) displays a negative trend with statistical significance at the 0.05 level.

Figure 8 illustrates the spatial distribution of spring vegetation density in two drought years, namely 2001 and 2018, as well as two wet years, namely 2007 and 2010. The central region of the watershed and the relatively flat terrain surrounding the cities of Varzaneh, Isfahan, and Zarinshahr, primarily comprising agricultural zones, exhibit the highest concentration of moderate (0.2-0.4) and good (0.4-0.6) vegetation class. Gradually, as one moves towards the mountains and elevations in the western and northwestern areas, the density of the vegetation diminishes. In these elevated regions, the most prevalent vegetation type is that of the poor category (0.1-0.2), which is predominantly found

in bushes and grasslands. Conversely, the eastern, north-eastern, southern, and southeastern segments of the basin are characterized by desert and arid regions, thereby showing a considerably lower vegetation density.

3.3. Relationship between *EVI* and the *SPI*

Figure 9 depicts the relationship between the *EVI* and the *SPI* during the spring season, this reflects the amount of rainfall in the Gavkhoni catchment area. The results reveal the statistically significant relationship between *EVI* and precipitation, as denoted by the significant correlation coefficient of R=0.5. Notably, the years 2001, 2008, and 2021 exhibit the lowest precipitation levels, with recorded values of 49.5, 32.26, and 37.4 mm, respectively, while the years 2007 and 2019 manifested the highest average rainfall during the period, reaching 133.9 and 116.96 mm, respectively. As can be seen in Fig. 9, during the years of scarce rainfall, vegetation cover experienced a decline, whereas the years with above-normal precipitation witnessed a rise in vegetation cover. As a consequence, it may be inferred that precipitation and soil moisture play a decisive role in modulating the fluctuations of *EVI* in the studied area. Specifically, the years 2001, 2008, and 2021, with their diminished vegetation coverage and areas spanning 1290.51, 1528.93, and 1783.42 km², respectively, experienced water stress-induced conditions that impacted vegetation. Conversely, the years 2007 and 2019 were characterized by heightened precipitation during the period, this fostered increases in vegetation, encompassing areas of 2158.58 and 2230.5 km², respectively.

One intriguing observation pertains to the springtime periods of 2011 and 2018, these were previously classified as dry years, with dry area percentages of 68.3 and 79.3, respectively. However, Fig. 10 reveals that during these two spring seasons, rainfall remained within the normal range. An analysis of the obtained data indicates that the average rainfall in the winter season of 2011 was 83.6 mm, which stood below the overall period’s average of 99.1 mm. Similarly, the spring season of 2018 produced an average rainfall of 63.7 mm, which was lower than the statistical average of 70.5 mm for the period. Moreover, during the winter season of 2018, the recorded rainfall not only fell below the average for the period but also deviated below the normal threshold. Additionally, it was previously noted

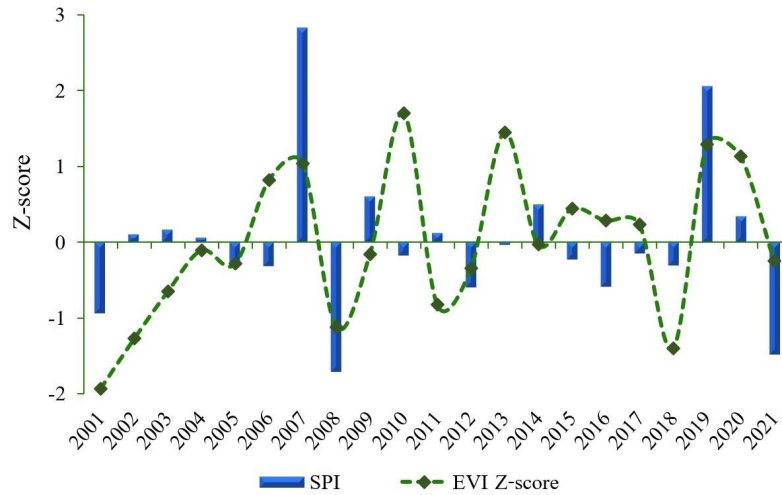


Fig. 9. Time series of the vegetation anomaly with the *SPI* anomaly in the spring season in the Gavkhouni catchment area 2001-2021.

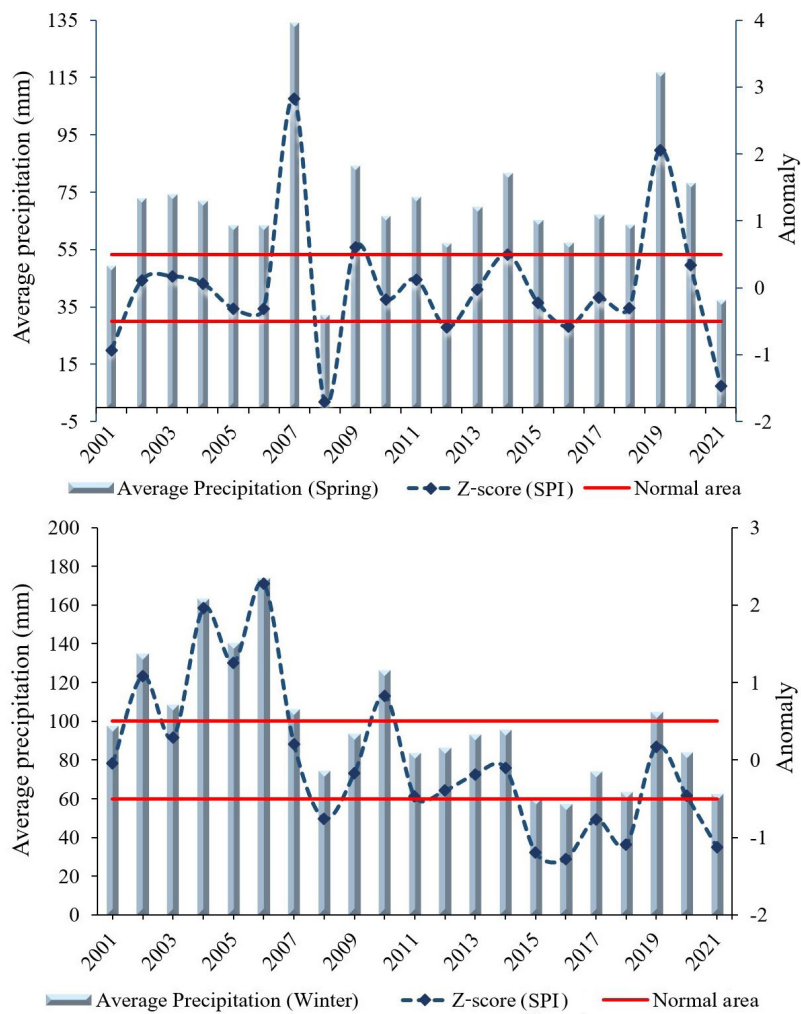


Fig. 10. Time series of precipitation and *SPI* changes in the spring and winter seasons in the Gavkhouni catchment area 2001-2021.

Table 4. Correlation matrix of *EVI* with precipitation in Gavkhoni catchment during the statistical period of 2001-2021

	<i>EVI</i>				
	Spring	Summer	Fall	Winter	Annual
Precipitation	0.47*	0.117	-0.167	0.112	-0.171

*Correlation significant at $p = 0.05$.

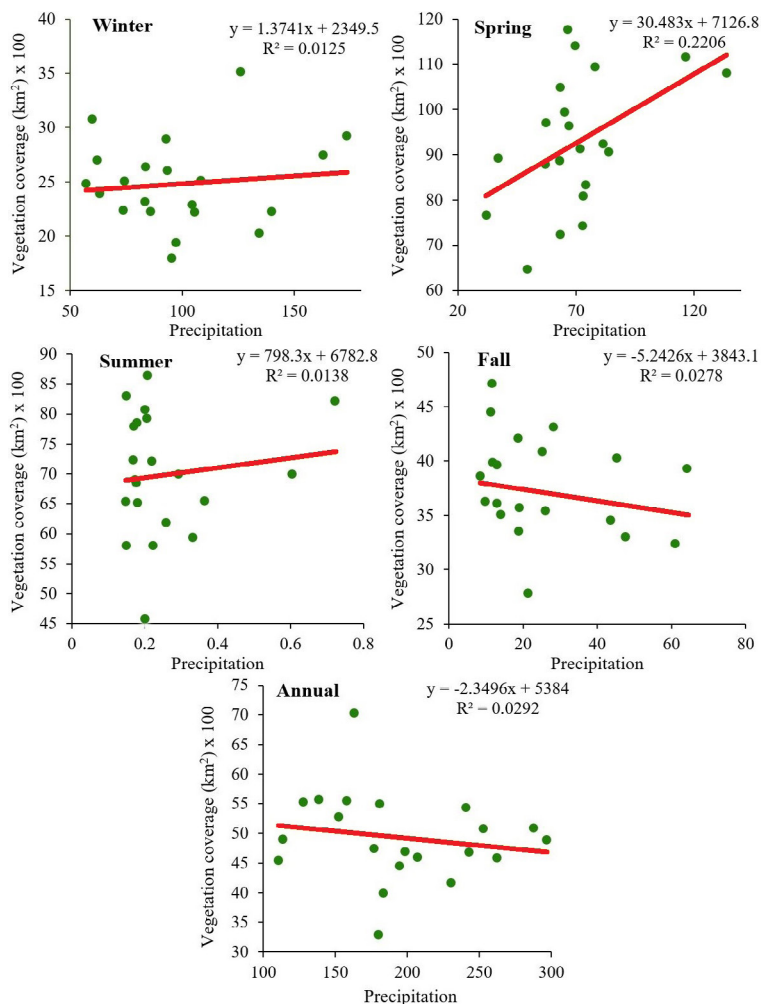


Fig. 11. Distribution of the total vegetation area for the four seasons and the annual rainfall in the Gavkhouni catchment area.

that the years 2010 and 2013 featured low dry percentages (21.4 and 12.6, respectively). However, upon closer examination of Figs 9 and 10, it is evident that the spring season of 2010 produced normal rainfall, while the winter season had rainfall levels that were almost normal and surpassed the normal threshold, which could have influenced the spring vegetation. Similarly, in 2013, both seasons produced a level of rainfall within the normal range, the substantial vegetation cover of 2277.9 km² which occurred during the spring season could have been influenced by other factors such as the temperature of the study area.

3.4. Comparison of annual and seasonal changes of vegetation with precipitation

Table 4 presents the correlation matrix between the *EVI* index and precipitation over a 21-year period. Remarkably, the spring vegetation area demonstrates a statistically significant correlation with precipitation at a significance level of 0.05. By contrast, the vegetation areas for summer, autumn, winter, and the entire annual period show no significant correlation with precipitation. Figure 11 highlights the distribution of precipitation levels concerning the corresponding vegetation areas. Apart from the spring vegetation area, all other seasonal and annual vegetation

areas exhibited no significant correlation with precipitation. Moreover, Table 5 provides insights into the seasonal and annual variations in vegetation cover within the study area, with particular consideration being focused on the delineation of wet and dry years during the spring season. These findings corroborate the observed percentage fluctuations in annual vegetation cover.

3.5. Results of the evaluation of cropland cover changes

Given the significance of agriculture within the study area, an independent investigation was conducted to assess the changes in agricultural land cover between the years 2001 and 2021. As the data presented in Table 6 shows, the years 2018, 2019, 2020, and 2021 stand out as having the smallest total crop cover area. This observation aligns with the outcomes presented in Table 2 and depicted in Fig. 7, where these years correspond to periods characterized by dry climatic conditions and a reduction in the extent of the vegetation. Conversely, the most extensive agricultural land coverage was observed during the years 2006, 2007, and 2010, this finding coincided with periods of the least pronounced drought within the studied statistical timeframe.

Table 5. Changes in the percentage of the total vegetation area of the four seasons and also annual changes in the Gavkhoni watershed 2001-2021

Year	Spring	Summer	Fall	Winter	Annual
2001	15.53	10.99	5.96	4.66	7.89
2002	17.85	14.86	8.06	4.86	9.58
2003	20.04	16.81	8.67	6.04	11.06
2004	21.95	18.73	9.82	6.60	11.76
2005	21.32	17.39	6.68	5.35	11.28
2006	25.20	19.95	9.68	7.03	12.24
2007	25.97	20.78	11.33	5.34	13.07
2008	18.40	13.94	8.58	6.03	10.92
2009	21.76	15.66	8.31	6.25	11.01
2010	28.29	19.07	10.7	8.45	16.88
2011	19.43	15.71	7.79	5.57	10.00
2012	21.12	17.33	9.54	5.35	11.24
2013	27.41	18.89	10.37	6.96	13.33
2014	22.21	15.74	8.51	4.32	10.68
2015	23.88	16.81	9.54	7.40	12.67
2016	23.31	16.58	9.28	5.97	13.40
2017	23.15	16.47	8.72	5.37	13.28
2018	17.39	14.26	7.93	5.75	11.39
2019	26.84	19.75	9.58	5.51	12.21
2020	26.30	19.42	10.12	6.33	13.21
2021	21.46	13.95	8.43	6.49	11.77

Table 6. Area of coverage of different *EVI* classes in the spring season of agricultural lands (km²) during the period of 2001-2021

Year	<i>EVI</i>				Total area
	0.1-0.2	0.2-0.4	0.4-0.6	> 0.6	
2001	215.44	717.888	77.38	1.00	1011.69
2002	233.81	743.56	106.31	1.38	1085.06
2003	201.38	900.19	254.38	3.38	1359.31
2004	204.69	911.38	373.19	7.50	1496.75
2005	205.06	1006.13	326.75	1.88	1539.81
2006	110.75	1018.56	564.81	7.44	1701.56
2007	214.25	1189.25	373.25	4.19	1780.94
2008	186.81	1260.81	242.5	1.13	1691.25
2009	256.25	1107.06	119.13	1.19	1483.63
2010	98.63	1191.5	294.06	2.63	1586.81
2011	295.06	885.5	79.75	1.00	1261.31
2012	233.06	894.81	82.75	0.56	1211.19
2013	156.69	849.31	107.38	1.75	1115.13
2014	167.25	759.75	86.44	2.25	1015.69
2015	127.44	775.31	160.63	3.13	1066.50
2016	117.06	758.88	215.56	4.25	1095.75
2017	153.13	775.06	121.06	2.19	1051.44
2018	190.5	582.38	53.38	1.00	827.25
2019	136.31	635.94	97.06	5.38	874.69
2020	113.25	664.75	171.13	1.88	951.00
2021	120.31	562.19	72.81	0.75	756.06
Average	177.96	866.2	189.51	2.66	1236.32

In Fig. 12, the changes in cropland cover during the spring season within the studied region, for the distinct *EVI* classes, are depicted. Across all classes, a negative trend is observed throughout the period spanning 2001 to 2021, with this decline becoming particularly pronounced from 2018 onwards. The findings presented in Table 7 reveal noteworthy insights. Specifically, *EVI* classes 0.1-0.2 and 0.2-0.4 showed a statistically significant and negative trend (at a significance level of 0.05), and the total annual area had a statistically significant and negative trend (at a significance level of 0.01). Conversely, for *EVI* classes 0.4-0.6 and >0.6 insignificant negative trends were observed.

3.6. Relationship between cropland cover changes and the *SPI*

In Table 7 the correlation coefficients between changes in distinct *EVI* classes for agricultural land cover and precipitation are presented. The findings indicate a significant correlation (at a significance level of 0.05) between winter precipitation and spring agricultural coverage. This implies that an augmentation in rainfall is associated with

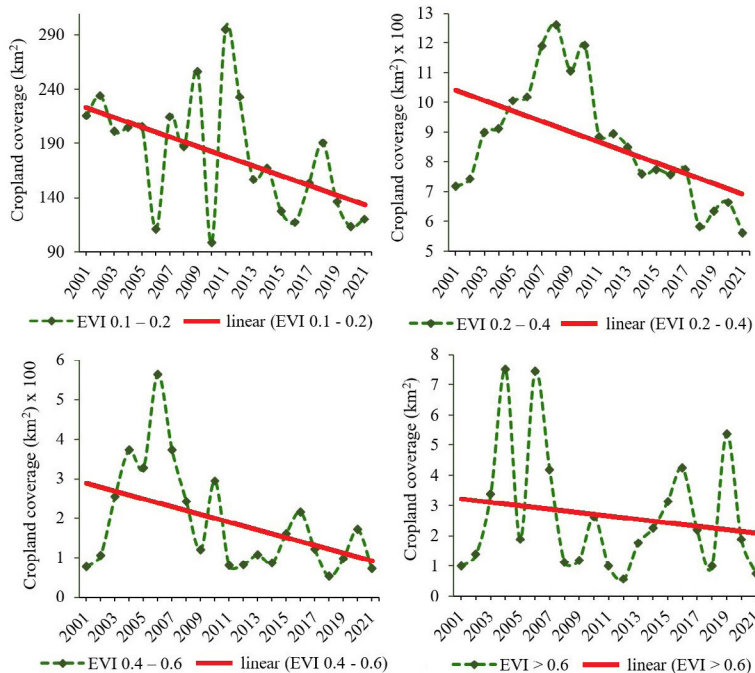


Fig. 12. Time series of different EVI classes for agricultural lands during the period of 2001-2021.

Table 7. Correlation of different classes of croplands during the statistical period of 2001-2021

	EVI				Total area
	0.1-0.2	0.2-0.4	0.4-0.6	> 0.6	
Year	-0.371*	-0.400*	-0.267	-0.077	-0.495**

Correlation significant at: *p = 0.05, **p = 0.01.

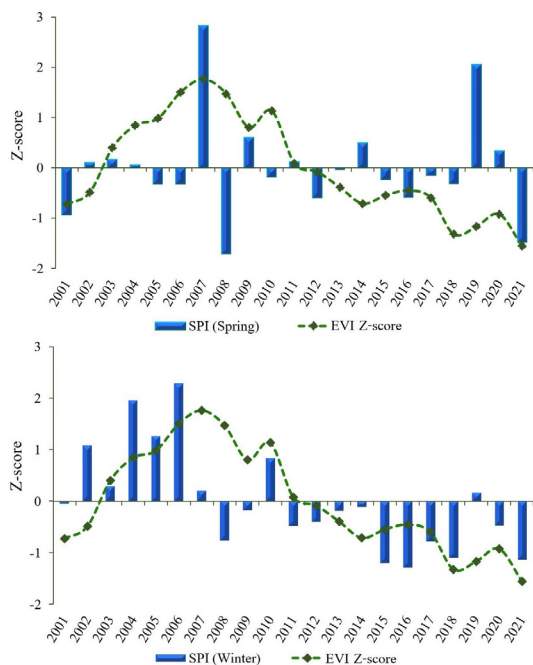


Fig. 13. Time series of the agricultural land cover anomaly and precipitation in spring and winter during the period 2001-2021.

an augmentation in vegetation cover. As illustrated in Fig. 13, a discernible pattern emerges wherein the reduction in precipitation during the winter season corresponds to a negative trend in agricultural land coverage within the Gavkhouni catchment region in the years from 2012 to 2021. During the spring season, although the trend may lack significance, a decrease in rainfall during this period aligns with reduced cropland coverage within the studied area.

4. DISCUSSION

This study focused on investigating the trends in vegetation areas and their correlation with precipitation in the Gavkhouni catchment area over a period of 21 years (2001-2021) using remote sensing data. The study region exhibited diverse vegetation patterns, with the northwest, west, parts of the southwest, and northeast being primarily characterized by pastures and lacking forest areas, which resulted in the prevalence of weak vegetation cover (0.1-0.2) in these regions. The maps of vegetation changes during the 21-year period and the Land Cover map of the Gavkhouni catchment area indicated that most of the area remained unchanged, thus signifying the absence of vegetation in these regions. However, certain parts, such as the northwest, certain areas in the centre, and limited regions in the northeast and southwest of the basin, experienced an upward trend in vegetation, while the central basin area and its extension towards the southwest and southeast exhibited a declining trend over the studied period which is consistent with the studies of Mirahsani *et al.* (2019). The investigation specifically focused on changes in vegetation areas during the spring seasons. Findings showed

that the years 2001, 2002, 2008, and 2018 had the lowest total spring vegetation area based on the *EVI*, with percentages of 15.53, 17.8, 18.39, and 17.3, respectively. By contrast, the years 2006, 2007, 2010, 2013, 2019, and 2020 exhibited the highest level of vegetation cover, with percentages of 25.19, 25.9, 28.2, 27.4, 26.8, and 26.3, respectively, in the total catchment area (41 552.3 km²). In the studies of Mahmoud *et al.* (2022) and Razipour (2019), the years 2001, 2008 and 2018 had the lowest level of spring vegetation and the years 2010 and 2019 had the highest. Furthermore, the *VCI* indicated that the highest dry area occurred in the years 2001, 2008, 2011, and 2018, with percentages of 83.4, 78.9, 68.3, and 79.3, respectively, of the total area. Conversely, the lowest percentage of drought was recorded in the years 2006, 2007, 2010, and 2013, with percentages of 23.1, 16.2, 21.4, and 12.6, respectively. The regions with the largest dry areas were identified in the north, northeast, east, southeast, and in certain parts of the centre, corresponding to cities such as Kuhpayeh, Antkhort, Mimeh, Izdtkhasht, Varzaneh, Alavijeh, and Dehgh. During dry conditions, the central and northwestern regions of the basin experienced almost normal conditions. The results produced by the central basin areas were primarily reliant on urban vegetation, forest parks in Isfahan, Zarinshahr, and Fouladshahr, and irrigated agricultural lands. Also, the northwest of the basin, benefiting from the presence of rivers and the Zayandeh Dam, showed a relatively higher vegetation cover as compared to other areas. The primary vegetation in this region was pasture and grassland, this was concentrated mainly in the highlands.

Further analysis revealed a significant correlation ($R=0.5$) between *EVI* and precipitation, indicating the existence of a significant relationship between the two parameters. Notably, the years 2001, 2008, and 2021 produced the lowest precipitation levels with 49.5, 32.26, and 37.4 mm, respectively, whereas the years 2007 and 2019 recorded the highest average rainfall with 133.9 and 116.96 mm, respectively, during the period. The observed vegetation cover aligned with these precipitation patterns, with the low rainfall years producing a decreased vegetation cover due to reduced soil moisture, leading to stress conditions for the vegetation. On the other hand, years with above-normal rainfall produced increased vegetation cover.

A statistical analysis revealed varying trends among the different vegetation classes based on the *EVI* achieved during the studied period. Specifically, an *EVI* range of 0.1 to 0.2 demonstrated a significantly increasing trend ($R=0.5$) during the spring season, with a confidence level of 95%. Conversely, poor (0.1 to 0.2) and moderate vegetation (0.2 to 0.4) exhibited a negative correlation with dry areas at a significance level of 0.01. The good vegetation (0.4 to 0.6) displayed a negative trend without significance, while the extensive vegetation class (above 0.6) exhibited a significant negative trend at a level of 0.05 which is consistent with the studies of Syed *et al.* (2021).

The findings of the study indicated a significant correlation ($R=0.5$) between *EVI* and precipitation, thereby highlighting the substantial relationship between these two parameters which is consistent with the studies of Rousta *et al.* (2020b). The years 2001, 2008, and 2021 produced the lowest rainfall with 49.5, 32.26, and 37.4 mm, respectively, while the years 2007 and 2019 recorded the highest average rainfall with 133.9 and 116.96 mm, respectively, throughout the period. As a consequence, the years characterized by a lower rainfall exhibited a decrease in vegetation cover, while the years with above-average precipitation witnessed higher vegetation levels. These results underscore the pivotal role of precipitation and soil moisture in influencing *EVI* variations in the studied region. The years 2001, 2008, and 2021 were marked by decreased levels of soil moisture due to insufficient rainfall, and exhibited the lowest coverage, which resulted in stressful conditions for vegetation across an area of 1 290.51, 1 528.93, and 1 783.42 km², respectively. Also, the decrease in precipitation in the winter and spring seasons from 2012 to 2021 caused a sharp decrease in crop area coverage, which is similar to the results achieved by Jafari and Hasheminasab (2017).

5. CONCLUSIONS

An important and noteworthy concern arises from the observed negative trend in vegetation coverage within the central region of the Gavkhouni catchment basin. This decline is particularly pronounced in densely populated urban areas, such as the metropolis of Isfahan, it is being driven by urbanization-induced population growth and construction activities. Also, a reduction in vegetation is evident in irrigated agricultural lands located in Zarinshahr and in the vicinity of Isfahan. The convergence of these factors has led to the erosion of ecological stability in these locations. A significant contributing factor is the diminishing water storage capacity in the Zayandeh-Roud dam, this was caused by reduced rainfall patterns and inefficiencies in water resource management. The root cause of the reduced vegetation is complex, it involves a combination of climatic, social, and cultural factors. Alongside urbanization and agricultural expansion, factors such as shifting climatic patterns, alterations in land use, and human activities have contributed to the decline in vegetation in the region. The repercussions of environmental instability are being manifested in various ways, including the onset of desertification, soil erosion, and climate change-related disruptions. The compounding effects of these factors will have profound economic, social, and climatic consequences, thereby underscoring the urgency of addressing these issues. The development of comprehensive strategies aimed at conserving and restoring vegetation cover in the Gavkhouni catchment basin are a necessity. In order to achieve this, integrated approaches that encompass sustainable land management, the optimization of water

resources, and urban planning measures must be implemented to mitigate any further degradation and safeguard the ecological equilibrium of the area. It is imperative to recognize the cascading effects of vegetation loss and also to adopt evidence-based policies to foster ecosystem resilience and sustainable development. Collaborative efforts among scientific communities, governmental bodies, and local stakeholders have the potential to create harmonious landscapes that balance human well-being with ecological vitality, thereby paving the way for a more prosperous and resilient future in the Gavkhouni catchment area.

Data Availability Statement: The data presented in this study are available on request from the first author.

Conflicts of Interest: The Authors do not declare any conflict of interest.

6. REFERENCES

- Ashraf M. and Routray J.K., 2013. Perception and understanding of drought and coping strategies of farming households in north-west Balochistan. *Int. J. Disaster Risk Reduction*, 5, 49-60. <https://doi.org/10.1016/j.ijdrr.2013.05.002>
- Belward A.S., Estes J.E., and Kline K.D., 1999. The IGBP-DIS global 1-km land-cover data set DISCover: A project overview. *Photogrammetric Engineering and Remote Sensing*, 65(9), 1013-1020.
- Bhuiyan C., Singh R., and Kogan F., 2006. Monitoring drought dynamics in the Aravalli region (India) using different indices based on ground and remote sensing data. *Int. J. Appl. Earth Obs. Geoinf.*, 8(4), 289-302. <https://doi.org/10.1016/j.jag.2006.03.002>
- Cancelliere A., Mauro G.D., Bonaccorso B., and Rossi G., 2007. Drought forecasting using the standardized precipitation index. *Water Res. Manag.*, 21, 801-819. <https://doi.org/10.1007/s11269-006-9062-y>
- Chang C.-T., Wang S.-F., Vadeboncoeur M.A., and Lin T.-C., 2014. Relating vegetation dynamics to temperature and precipitation at monthly and annual timescales in Taiwan using MODIS vegetation indices. *Int. J. Remote Sens.*, 35(2), 598-620. <https://doi.org/10.1080/01431161.2013.871593>
- Couteron P., Hunke P., Bellot J., Estrany J., Martínez-Carreras N., Mueller E.N., Papanastasis V.P., Parmenter R.R., and Wainwright J., 2014. Characterizing patterns. In: *Patterns of Land Degradation in Drylands: Understanding Self-Organised Ecogeomorphic Systems*. 211-245. Springer Science+Business Media Dordrecht. <https://doi.org/10.1007/978-94-007-5727-1>
- Dikici M., 2022. Drought analysis for the Seyhan Basin with vegetation indices and comparison with meteorological different indices. *Sustainability*, 14(8), 4464. <https://doi.org/10.3390/su14084464>
- Dorjsuren M., Liou Y.-A., and Cheng C.-H., 2016. Time series MODIS and in situ data analysis for Mongolia drought. *Remote Sensing*, 8(6), 509. <https://doi.org/10.3390/rs8060509>
- Farahani A., Eftekhari A., Mirdavoudi H., and Goudarzi G., 2022. The effect of enclosure and climate changes on vegetation characteristics in the saline habitats of Meyghan playa margin, Arak. *Iran. J. Seed Res.*, 29(3), 201-210. <https://doi.org/10.22092/ijdr.2022.127631>
- Farajzadeh M., Fathnia A., Alijani B., and Zaeian P., 2011. Assessment of the effect of climatic factors on the growth of dense pastures of Iran, Using AVHRR Images. *Physical Geography Research Quarterly*, 43(75(1390)), 491307.
- Ghafarian Malamiri H.R., Rousta I., Olafsson H., Zare H., and Zhang H., 2018. Gap-filling of MODIS time series land surface temperature (LST) products using singular spectrum analysis (SSA). *Atmosphere*, 9(9), 334. <https://doi.org/10.3390/atmos9090334>
- Gupta A., Moniruzzaman M., Hande A., Rousta I., Olafsson H., and Mondal K.K., 2020. Estimation of particulate matter (PM_{2.5}, PM₁₀) concentration and its variation over urban sites in Bangladesh. *SN Applied Sciences*, 2(12), 1993. <https://doi.org/10.1007/s42452-020-03829-1>
- Hansen M.C., DeFries R.S., Townshend J.R., and Sohlberg R., 2000. Global land cover classification at 1 km spatial resolution using a classification tree approach. *Int. J. Remote Sens.*, 21(6-7), 1331-1364. <https://doi.org/10.1080/014311600210209>
- Huete A., Didan K., Miura T., Rodriguez E.P., Gao X., and Ferreira L.G., 2002. Overview of the radiometric and biophysical performance of the MODIS vegetation indices. *Remote Sens. Environ.*, 83(1-2), 195-213. [https://doi.org/10.1016/S0034-4257\(02\)00096-2](https://doi.org/10.1016/S0034-4257(02)00096-2)
- Huete A., Justice C., and Liu H., 1994. Development of vegetation and soil indices for MODIS-EOS. *Remote Sens. Environ.*, 49(3), 224-234. [https://doi.org/10.1016/0034-4257\(94\)90018-3](https://doi.org/10.1016/0034-4257(94)90018-3)
- Huete A., Justice C., and van Leeuwen W., 1999. MODIS vegetation index (MOD 13) algorithm theoretical basis document, version 3. University of Arizona, 129p.
- Huete A., Liu H., Batchily K., and Van Leeuwen W., 1997. A comparison of vegetation indices over a global set of TM images for EOS-MODIS. *Remote Sensing of Environ.*, 59(3), 440-451. [https://doi.org/10.1016/S0034-4257\(96\)00112-5](https://doi.org/10.1016/S0034-4257(96)00112-5)
- Jafari R. and Bakhshandehmehr L., 2016. Quantitative mapping and assessment of environmentally sensitive areas to desertification in central Iran. *Land Degradation Development*, 27(2), 108-119. <https://doi.org/10.1002/ldr.2227>
- Jafari R. and Hasheminasab S., 2017. Assessing the effects of dam building on land degradation in central Iran with Landsat LST and LULC time series. *Environmental Monitoring and Assessment*, 18, 1-15. <https://doi.org/10.1007/s10661-017-5792-y>
- Kafarski M., Majcher J., Wilczek A., Szyplowska A., Lewandowski A., Zackiewicz A., and Skierucha W., 2019. Penetration depth of a soil moisture profile probe working in time-domain transmission mode. *Sensors*, 19(24), 5485. <https://doi.org/10.3390/s19245485>
- Kogan F.N., 1995. Droughts of the late 1980s in the United States as derived from NOAA polar-orbiting satellite data. *Bull. Am. Meteorol. Soc.*, 76(5), 655-668. [https://doi.org/10.1175/1520-0477\(1995\)076<0655:DOTLIT>2.0.CO;2](https://doi.org/10.1175/1520-0477(1995)076<0655:DOTLIT>2.0.CO;2)
- Kogan F.N., 1997. Global drought watch from space. *Bull. Am. Meteorol. Soc.*, 78(4), 621-636. [https://doi.org/10.1175/1520-0477\(1997\)078<0621:GDWFS>2.0.CO;2](https://doi.org/10.1175/1520-0477(1997)078<0621:GDWFS>2.0.CO;2)

- Khosravi Yeganeh S., Karampour M., and Nasiri B., 2023. Evaluation of the effect of drought on vegetation in Iran using satellite images and meteorological data. *Iranian J. Remote Sensing GIS*. <https://doi.org/10.48308/gisj.2023.103394>
- Loveland T.R. and Belward A., 1997. The international geosphere biosphere programme data and information system global land cover data set (DISCover). *Acta Astronautica*, 41(4-10), 681-689. [https://doi.org/10.1016/S0094-5765\(98\)00050-2](https://doi.org/10.1016/S0094-5765(98)00050-2)
- Luan J., Liu D., Zhang L., Huang Q., Feng J., Lin M., and Li G., 2018. Analysis of the spatial-temporal change of the vegetation index in the upper reach of Han River Basin in 2000-2016. *Proc. Int. Association of Hydrological Sciences*, 379, 287-292. <https://doi.org/10.5194/piahs-379-287-2018>
- Mahmood S.A.R., Rosta I., and Mazidi A., 2022. Investigating the sustainability of vegetation change trends using remote sensing (Case Study: Northern River Basin of Afghanistan). *Geography and Environmental Sustainability*, 12(2), 17-35. <https://doi.org/10.22126/GES.2022.7416.2496>
- Majcher J., Kafarski M., Wilczek A., Szyplowska A., Lewandowski A., Woszczyk A., and Skierucha W., 2021. Application of a dagger probe for soil dielectric permittivity measurement by TDR. *Measurement*, 178, 109368. <https://doi.org/10.1016/j.measurement.2021.109368>
- Manesh M., Alamdarlo E.H., and Jazi N.A., 2018. Assessing the reclamation and destruction of vegetation using remote sensing (Case Study: Tehran Province). *Int. Conf. Society Environment, Tehran*. <https://civilica.com/doc/815877/>
- Mansourmoghaddam M., Ghafarian Malamiri H.R., Rosta I., Olafsson H., and Zhang H., 2022. Assessment of Palm Jumeirah Island's construction effects on the surrounding water quality and surface temperatures during 2001-2020. *Water*, 14(4), 634. <https://doi.org/10.3390/w14040634>
- Martiny N., Camberlin P., Richard Y., and Philippon, N., 2006. Compared regimes of NDVI and rainfall in semi-arid regions of Africa. *Int. J. Remote Sensing*, 27(23), 5201-5223. <https://doi.org/10.1080/01431160600567787>
- Mirahsani M., Salman Mahiny A., Soffianian A., Moddares R., Jafari R., and Mohammadi J., 2018. Evaluation of vegetation supply water index through time-series images of MODIS products in drought monitoring over Gavkhuni Basin. *Iranian J. Applied Ecology*, 6(4), 31-47. <https://doi.org/10.29252/ijae.6.4.31>
- Mirahsani M.S., Salman Mahiny A., Soffianian A., Mohamadi J., Modarres R., Modares R., and Pourmanafi S., 2019. Evaluation of trend in vegetation variations using time series images and Mann-Kendall test over Gavkhuni Basin. *J. Environmental Studies*, 45(1), 99-114. <https://doi.org/10.22059/jes.2019.260567.1007699>
- Olafsson H. and Rosta I., 2021. Influence of atmospheric patterns and North Atlantic Oscillation (NAO) on vegetation dynamics in Iceland using Remote Sensing. *Remote Sens. Environ.*, 54(1), 351-363. <https://doi.org/10.1080/22797254.2021.1931462>
- Pei F., Wu C., Liu X., Li X., Yang K., Zhou Y., Wang K., Xu L., and Xia G., 2018. Monitoring the vegetation activity in China using vegetation health indices. *Agric. Forest Meteorology*, 248, 215-227. <https://doi.org/10.1016/j.agrformet.2017.10.001>
- Peng J., Liu Z., Liu Y., Wu J., and Han Y., 2012. Trend analysis of vegetation dynamics in Qinghai-Tibet Plateau using Hurst Exponent. *Ecological Indicators*, 14(1), 28-39. <https://doi.org/10.1016/j.ecolind.2011.08.011>
- Peters E., 2003. Propagation of drought through groundwater systems: illustrated in the Pang (UK) and Upper-Guadiana (ES) catchments. Ph.D. Thesis, Wageningen University, The Netherlands.
- Rannow S. and Neubert M., 2014. Managing protected areas in central and eastern Europe under climate change. In: Springer, Cham., <https://doi.org/10.1007/978-94-007-7960-0>
- Raynolds M.K., Comiso J.C., Walker D.A., and Verbyla D., 2008. Relationship between satellite-derived land surface temperatures, arctic vegetation types, and NDVI. *Remote Sens. Environ.*, 112(4), 1884-1894. <https://doi.org/10.1016/j.rse.2007.09.008>
- Razipoor M.E., 2019. Assessing the vegetation condition of herat province, Afghanistan Using GIS. *Appl. Geol. Geophysics*, 7(4), 92-97. <https://doi.org/10.9790/0990-0704019297>
- Rosta I., Javadizadeh F., Dargahian F., Olafsson H., Shiri-Karimvandi A., Vahedinejad S.H., Doostkamian M., Monroy Vargas E.R., and Asadolahi A., 2018. Investigation of vorticity during prevalent winter precipitation in Iran. 2018, 6941501. <https://doi.org/10.1155/2018/6941501>
- Rosta I., Khosh Akhlagh F., Soltani M., and Modir Taheri Sh S., 2014. Assessment of blocking effects on rainfall in north-western Iran. *Proceedings of COMECAP 2014*, p.291.
- Rosta I., Mahmood S.R., and Saberi M.A., 2020a. Investigation of vegetation change using NDVI index and MODIS sensor in Balkh province of Afghanistan (in Persian). 2nd Nat. Conf. New Thoughts and Technologies in Geographical Sciences, Zanjan: Zanjan University.
- Rosta I., Olafsson H., Moniruzzaman M., Zhang H., Liou Y.-A., Mushore T.D., and Gupta A., 2020b. Impacts of drought on vegetation assessed by vegetation indices and meteorological factors in Afghanistan. *Remote Sens.*, 12(15), 2433. <https://doi.org/10.3390/rs12152433>
- Rosta I., Nasserzadeh M.H., Jalali M., Haghghi E., Olafsson H., Ashrafi S., Doostkamian M., and Ghasemi, A., 2017. Decadal spatial-temporal variations in the spatial pattern of anomalies of extreme precipitation thresholds (Case Study: Northwest Iran). *Atmosphere*, 8(8), 135. <https://doi.org/10.3390/atmos8080135>
- Saraei S., Afrakhteh H., Riahi V., and Jalalian H., 2017. Evaluate the usage of information and communication technology in agricultural water use optimization using soft system approach. *Interdisciplinary Studies in Humanities*, 9(4), 49-70. <https://doi.org/10.22631/isi/h.2017.1936.2479>
- Shah R., Bharadiya N., and Manekar V., 2015. Drought index computation using standardized precipitation index (SPI) method for Surat District, Gujarat. *Aquatic Procedia*, 4, 1243-1249. <https://doi.org/10.1016/j.aqpro.2015.02.162>
- Syed A., Liu X., Moniruzzaman M., Rosta I., Syed W., Zhang J., and Olafsson H., 2021. Assessment of climate variability among seasonal trends using in situ measurements: A case study of Punjab, Pakistan. *Atmosphere*, 12(8), 939. <https://doi.org/10.3390/atmos12080939>

- Tate E., and Gustard A., 2000. Drought definition: a hydrological perspective. In: *Drought and drought mitigation in Europe*, 23-48. Springer. https://doi.org/10.1007/978-94-015-9472-1_3
- Wan Z., Wang P., and Li X., 2004. Using MODIS land surface temperature and normalized difference vegetation index products for monitoring drought in the southern Great Plains, USA. *Int. J. Remote Sens.*, 25(1), 61-72. <https://doi.org/10.1080/0143116031000115328>
- Weishou S., Di J., Hui Z., Shouguang Y., Haidong L., and Naifeng L., 2011. The response relation between climate change and NDVI over the Qinghai-Tibet plateau. *J. World Academy of Science, Eng. Technology*, 59, 2216-2222. <https://doi.org/10.5281/zenodo.1055110>
- Zhang N., Hong Y., Qin Q., and Zhu L., 2013. Evaluation of the visible and shortwave infrared drought index in China. *Int. J. Disaster Risk Science*, 4, 68-76. <https://doi.org/10.1007/s13753-013-0008-8>
- Zhong L., Ma Y., Salama M.S., and Su Z., 2010. Assessment of vegetation dynamics and their response to variations in precipitation and temperature in the Tibetan Plateau. *Climatic Change*, 103(3-4), 519-535. <https://doi.org/10.1007/s10584-009-9787-8>